Applied Surface Science 714 (2025) 164456

Contents lists available at ScienceDirect

Applied Surface Science

journal homepage: www.elsevier.com/locate/apsusc

Full Length Article

Temperature-assisted high-energy-per-atom argon cluster SIMS of layered hybrid nanomaterials

Giuseppe Ragusano [a], Valentina Spampinato [a,*], Alessandro Auditore [a], Nunzio Tuccitto [a], Marta Penconi [b,c,*], Alberto Bossi [b,c], Alexis Franquet [d], Thierry Conard [d], Antonino Licciardello [a]

[a] Department of Chemical Sciences, University of Catania, Viale A. Doria 6, 95125 Catania, Italy
[b] Istituto di Scienze e Tecnologie Chimiche "Giulio Natta" del Consiglio Nazionale delle Ricerche, CNR-SCITEC, via Fantoli 16/15, 20138 Milano, Italy
[c] SmartMatLab Centre, via Golgi 19, 20133 Milano, Italy
[d] IMEC, Kapeldreef 75, Leuven 3001, Belgium

ARTICLE INFO

Keywords:
Time-of-flight secondary ion mass spectrometry
Argon cluster depth profile
Molybdenum oxide
Arylamine
Hybrid nanomaterials
Temperature-assisted depth profile

ABSTRACT

Time of Flight Secondary Ion Mass Spectrometry is a powerful technique for the characterization of various materials. Depth profiling in the dual beam mode enables the acquisition of information about the three-dimensional composition of a sample. In this context, the selection of the most appropriate sputter conditions is of critical importance in order to ensure the reliability of the results obtained. Despite advancements, challenges persist in finding a suitable sputter source to perform depth profiling on hybrid nanomaterials (based on the mixing of pure organic and inorganic compounds), primarily due to the different sputtering conditions required for the inorganic and the organic components. In this work, we present an approach that employs a high-energy-per-atom argon cluster sputter source to perform depth profiling of a model hybrid sample consisting of molybdenum oxide and N,N′-Di(1-naphthyl)-N,N′-diphenyl-(1,1′-biphenyl)-4,4′-diamine. The findings demonstrated that decreasing the cluster size while maintaining a high kinetic energy of the beam allowed to increase the sputtering yield for the inorganic moiety, while preserving the molecular information of the organic counterpart. Moreover, we demonstrated that damage accumulation and ion beam mixing processes can be successfully attenuated by decreasing the sample temperature during depth profiling.

1. Introduction

Organic-inorganic hybrid nanostructures represent a significant advancement in materials science with the potential to revolutionize a wide range of high-tech applications [1]. In particular, combining organic and inorganic semiconductors in the form of thin layers, in either a planar structure or bulk structure, offers a way to prepare new functional materials for next-generation optoelectronic devices. This approach couples the stability and high carrier mobilities of the inorganic material with the cost-effectiveness, ease of production, tunability, and flexibility of the organic material.

Organic-inorganic hybrid materials are currently exploited as planar heterostructure in several types of optoelectronic devices, such as solar cells, light-emitting diodes, and photodetectors, based on layered thin films where interfaces between materials with different electronic properties are responsible for charge management (generation, injection, transport and blocking).

Hybrid materials further exhibit additional properties that are not present in their constituent components. For example, inorganic–organic heterojunctions between a donor and an acceptor material have recently demonstrated to be able to produce sub-band gap light absorption at the interface, resulting in a photoresponsive material for application in near infrared (NIR) photodetectors [2,3].

The development of hybrid layered materials with well-defined interfaces and optimized morphologies is essential for enhancing their functional properties. The physico-chemical interactions at these interfaces play a critical role in determining overall performance. However, complex phenomena such as aging [4], diffusion, [5] and degradation processes [6,7] can affect the long-term stability and efficiency of these heterostructures. Therefore, a thorough understanding of

* Corresponding authors.
E-mail addresses: valentina.spampinato@unict.it (V. Spampinato), marta.penconi@cnr.it (M. Penconi).

https://doi.org/10.1016/j.apsusc.2025.164456
Received 24 June 2025; Received in revised form 11 August 2025; Accepted 27 August 2025
Available online 28 August 2025

their structural characteristics and time-dependent behavior is vital. Achieving this requires the use of advanced characterization techniques capable of probing their internal architecture in detail.

Time-of-Flight Secondary Ion Mass Spectrometry (ToF-SIMS) is a highly effective tool for the compositional and structural analysis of a wide variety of materials. Its capacity to provide three-dimensional, spatially resolved chemical information by means of its depth profiling and imaging capability has resulted in advancements in the physico-chemical characterization of technological devices. However, a significant challenge lies in identifying operational conditions to enable the simultaneous profiling of inorganic materials, which require high-impact energies, and organic materials, which necessitate a balance between energy and mass of the primary ion to preserve molecular integrity and prevent damage accumulation.

Historically, secondary ion mass spectrometry depth profiling has been employed to characterize samples in the microelectronics industry, focusing on inorganic materials (metals, semiconductors, and oxides) involving the use of monoatomic ion sources such as Ar^+, O^+ and Cs^+, at kinetic energies within the kiloelectronvolt (keV) range [8].

The sputtering process, on which SIMS is based, is inherently destructive, resulting in the generation of artifacts due to ion beam-sample interactions. Specifically, the high fluences of the primary ion beam necessary for sputtering can lead to accumulation of damage during profiling, including morphological evolution [9], radical generation [9,10], ion beam mixing [11] and preferential sputtering [12–14]. Indeed, when performing depth profiling with monoatomic beams on an organic or – polymeric materials, damage accumulation was observed on the surface [9,10,15–17].

As demonstrated by Noël et al., [18] the utilization of a low energy Cs^+ sputter beam allowed to achieve favourable outcomes in profiling hybrid materials. Cesium has been shown to act as a radical scavenger [19,20], reducing radical recombination in organic materials and preserving molecular information, while maintaining its capacity to erode inorganic materials effectively [21]. Despite this, for certain organic structures, Cs^+ still leads to a loss of chemical information and the absence of a well-defined steady state for characteristic fragments [22–24]. This issue can be particularly significant in instances where multiple organic layers are deposited sequentially, thereby complicating the identification of the precise nature of each component within the investigated sample.

The advent of polyatomic (or cluster) ion sources has led to significant advancements in the field of probing organic materials, overcoming the limitation arising from damage accumulation and loss of molecular information. Upon impact with the sample surface, each atomic component of the cluster acquires a fraction of the total cluster energy, leading to a reduction in the projected range of the ion in the sample. Moreover, due to the time- and space- overlap of the trajectories of each individual component of the cluster, energy is more evenly distributed within the interaction volume. All above results, among others, in a significant reduction of damage accumulation in the sample during depth profile measurements [25]. Starting from SF_5^+ [15,17,25], moving to C_{60}^+ [26–28], and ultimately to Ar_n^+ clusters [29–38], the quality of depth profiles of organic materials has improved, enabling the tracking of repeating unit fragments from polymers and entire molecular ions and large fragments from organic solids. Nonetheless, the identification of optimal sputter conditions for the acquisition of depth profiling on hybrid devices remains an ongoing challenge within the SIMS community.

Shen et al. [39] tried C_{60}^+ as sputter beam in dual beam depth profiling of a hybrid sample composed of a gold delta layer between thicker cholesterol layers, resulting in ion beam enhanced gold diffusion and subsequent damage accumulation through the cholesterol buried layer, with lower signal intensities compared with the upper layer.

Argon Gas Cluster Ion Beams (Ar-GCIB) are generally employed for the investigation of organic solids and polymeric materials, leading to high sputtering yields, low damage accumulation, and sharper molecular depth profiles [29,30]. The lower energy per atom, combined with the great number of atoms impacting the surface, creates large craters with negligible damage accumulation, from which a significant number of molecular fragments are ejected [31]. Although Ar-GCIB has been extensively utilized for the investigation of organic matter, its application in the study of inorganic materials has been relatively limited [32–36].

Seah [35] showed that the dependance of sputtering yield on both energy and size of the cluster projectile for various materials can be described using a "universal" equation. This equation relates the sputtering yield to the energy per atom of the cluster, using two fitting parameters (A and q). Interestingly, the sputtering yields of different inorganic materials tend to collapse roughly in the same curve, which differs from the curve onto which the data for organic materials approximately converge.

The study further highlights that, under conditions most suited for organics (E/n from 2 to 5 eV), the sputter yields of inorganic materials are between 2 and 3 orders of magnitude lower than those of organic materials, which makes it difficult to erode thick inorganic layers usually present in hybrid devices or composites.

Nevertheless, the difference in sputter yields between organic and inorganic materials tends to diminish as the E/n ratio increases and the clusters become smaller, particularly under conditions where organic materials are prone to damage accumulation. A potential compromise could involve utilising Argon clusters with $\leq$ 500 atoms and energy $\geq$ 10 keV, which are capable of inflicting minimal damage to organics while concurrently enhancing the sputter yields of inorganic materials [40].

Finally, it has been demonstrated for both monoatomic and polyatomic sources that temperature significantly affects depth profiling outcomes on organic and polymeric systems [28,37,38], resulting in decreased sputter-induced roughness evolution, improved depth resolution, and higher overall structure-related signals compared to analyses conducted at room temperature [37,38].

In particular, Mahoney et al. [38] proposed that the improved depth profile characteristics at low temperatures for polymers are attributable to changes in polymer properties, which enhance inter and intrachain coupling, resulting in more uniform sputtering. Another explanation could be the reduced cross-linking tendency during sputtering at low temperatures, which minimizes chemical damage and allow to preserve the structural integrity of characteristic fragments [28,41,42].

Therefore, the effect of the temperature on the depth-profiling could be exploited to further improve the results obtained at room temperature in those cases where the organic component is severely affected by beam-induced damage.

This study investigates the potential of using *a high-energy-per-atom argon cluster* sputtering beam for the depth profiling of a model layered hybrid system obtained by vacuum thermal deposition of two materials that are already used in optoelectronic devices: molybdenum trioxide (MoO_3), which is usually used as a acceptor and buffer layer, and N,N′-Di(1-naphthyl)-N,N′-diphenyl-(1,1′-biphenyl)-4,4′-diamine (NPD, Fig. 1a), which is an arylamine commonly used as a hole transport and donor material. Furthermore, the realized organic–inorganic interface has been proven to produce a NIR photoresponsive material demonstrating the potential of this hybrid architecture for NIR photodetection [2,3]. To investigate how variations in E/n influence the quality of the resulting data, two extreme conditions were employed: Ar_{4000}^+ 20 keV (5 eV/n), which is typically utilized for depth profiling organic materials, and *high-energy-per-atom* Ar_{500}^+ 20 keV (40 eV/n). Initially, depth profiles were acquired on two single-component thin films (amine and oxide) to determine which sputter condition was the best compromise between eroding the inorganic component and preserving information on the organic one. Then, depth profiles were acquired on a layered hybrid system consisting of the above-mentioned materials. Additionally, temperature-assisted depth profiling was conducted to investigate how reduced sample temperature affects the

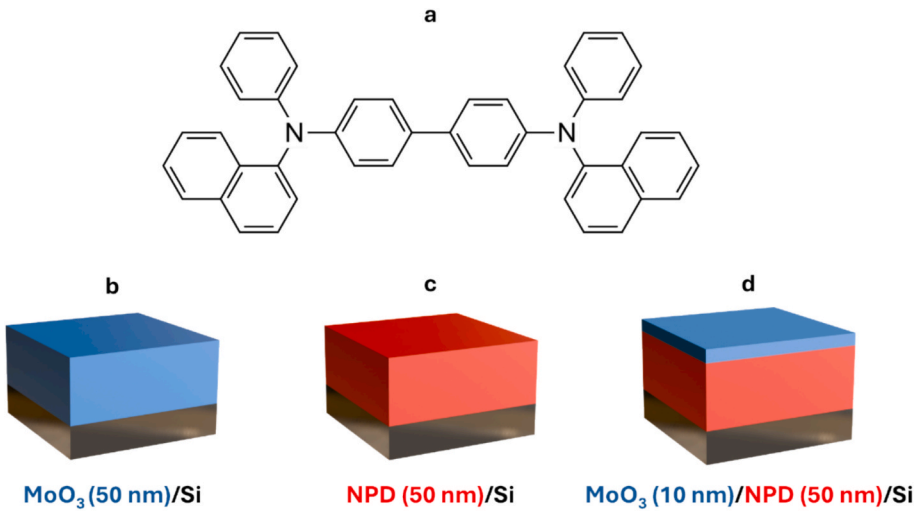

Fig. 1. Molecular structure of the organic donor material and layout of thin film architectures; a) NPD, b) MoO_3 film on Si, 50 nm thickness, c) NPD film on Si, 50 nm thickness, d) MoO_3/NPD film on Si, 10 nm and 50 nm thickness respectively.

preservation of molecular information from characteristic organic fragments. This study aims to contribute to the development of an effective methodology for the physico-chemical characterization of hybrid devices in order to obtain detailed information on such complex systems.

2. Materials and methods

2.1. Sample preparation

A commercially available arylamine, NPD (N,N′-Di(1-naphthyl)-N, N′-diphenyl-(1,1′-biphenyl)-4,4′-diamine) (Fig. 1a), was purchased from TCI and utilized as received to serve as the organic component of the hybrid material. For the inorganic component, molybdenum trioxide (MoO_3), (Merck) was employed. Thin films were prepared on silicon substrates which were cleaned prior depositions by successive sonication with deionized water, acetone, and isopropanol for 10 min each.

The samples were prepared by physical vapor deposition at a pressure of 2×10^{-6} mbar in a Kenosistec KE-500 chamber. NPD was evaporated from an effusive Knudsen cell source and MoO_3 from a thermal Joule effect source. The sample holder was located 300 mm away from the sources and maintained at room temperature. A quartz-crystal microbalance, positioned close to the sample and equipped with gold-coated crystal sensor (INFICON), allowed for monitoring the deposition rates (0.30 Å/s for NPD and 0.15 Å/s for MoO_3).

The nominal thickness of NPD and MoO_3 layers was determined by correlating the reading of the quartz crystal monitor to the measured thickness as obtained by a Bruker DektakXT contact profilometer, for at least three evaporated films of each material.

Three distinct samples (Fig. 1b, c, d) were systematically prepared on silicon substrate, respectively: 50 nm MoO_3 layer, 50 nm NPD layer and 10 nm MoO_3/50 nm NPD layers.

2.2. ToF-SIMS measurements

ToF-SIMS depth profiles of the fabricated samples were acquired using a ToF-SIMS IV instrument (IONTOF, GmbH, Münster, Germany) retrofitted with an Ar-GCIB source and equipped with a temperature-controlled sample holder for low-temperature depth profiling (using liquid nitrogen). A ToF-SIMS NCS instrument (ION-TOF GmbH, Münster, Germany) on which an Atomic Force Microscope (AFM) is integrated in the same UHV analysis chamber was used for in-situ AFM measurements. Both instruments operated in dual beam mode, utilizing a liquid metal ion gun (LMIG) for analysis and an Ar-GCIB source for sputtering.

For the LMIG analysis beam, Bi_3^+ clusters at 25 keV were selected, with a primary ion current between 0.2 and 0.3 pA, measured by a Faraday cup. The beam was rastered over areas of 200×200 μm^2.

For the Ar-GCIB source, two sputter conditions with different cluster distributions were employed: Ar_{500}^+ at 20 keV and Ar_{4000}^+ at 20 keV. In both conditions, the sputter beam current was 0.2 nA, rastered over a surface of 500×500 μm^2. Depth profiling was conducted in "non-interlaced" mode, with a cycle time of 200 μs, utilizing 1 frame of analysis and 1 frame of sputtering, and a 0.5-second pause.

The spectra, acquired in positive polarity mode, were calibrated using the following ions: CH_3^+, $C_3H_7^+$, $C_4H_3^+$ and $C_6H_5^+$.

2.3. XPS measurements

X-ray Photoelectron Spectroscopy (XPS) analysis was performed using a VersaProbe 3 instrument (Physical Electronics), equipped with a monochromatic Al Kα X-ray source (photon energy: 1486.6 eV) utilizing a spot size of 100 μm. Charge neutralization was applied throughout the measurements to compensate for surface charging. Sputter depth profiling was carried out using an argon gas cluster ion beam (Ar-GCIB) source, with a cluster size distribution centered at 620 atoms and an acceleration voltage of 20 keV. The selected primary ion current was 8.0 nA. The ion beam was rastered over a 3×3 mm^2 area. All spectra were acquired at an emission angle of 45° relative to the sample surface. Binding energy calibration was referenced to the C 1 s peak at 284.8 eV.

2.4. AFM measurements

Topography images and long-range surface profiles on the sputtered craters were acquired in-situ with the AFM module integrated into the same UHV analysis chamber of the ToF-SIMS NCS [43]. The images were obtained in contact mode using a diamond tip on a scanned area of 10×10 μm^2 (scan rate of 5 μm/s, 256×256 pixels).

2.5. Sputtering yields

The sputtering yields of the investigated samples were determined using two single-component thin films. Depth profiling was halted at approximately half the film thickness, after which a long-range surface scan (acquired in-situ with the AFM module) was conducted over each crater region to measure its depth. This approach enabled the calculation of the sputtering yield using Equation (1) [18]:

$$Y = \frac{eAd}{It} \quad (1)$$

Equation (1): Sputtering yield equation.

where e is the electron charge (1.6e-19 C), A is the surface area of the sputtered crater (nm^2), d is the measured crater depth (nm), I is the sputter current as an average value between the currents measured before and after the depth profile (A), and t is the sputtering time (s).

3. Results and discussion

The present study focuses on the evaluation of the exploitation of a high-energy-per-atom argon cluster sputtering beam for the depth profiling of layered hybrid materials. As outlined in the introduction, the ideal sputtering conditions for organic and inorganic materials may differ significantly, necessitating the identification of a satisfactory compromise in experimental conditions to achieve the desired outcome. With this aim, two Ar-GCIB sputtering conditions were used: an Ar^+_{4000} 20 keV (5 eV/n) was selected as an appropriate condition for eroding organic materials, and an Ar^+_{500} 20 keV (40 eV/n) beam was used with the aim of evaluating the effect of an increase of E/n value on the sputtering of both inorganic and organic materials. The investigation focused on sputtering yield (Y), retention of molecular information and ion beam-induced roughness evolution. Y quantifies the volume (nm^3) of sample eroded per incident primary ion (PI), serving as a key measure of sputter beam efficiency. Furthermore, the evolution of roughness is of critical importance as it impacts the depth resolution of the acquired data. Indeed, due to the presence of roughness, secondary ions may originate simultaneously from differing heights of the sample, thereby complicating data interpretation, including the accurate definition of interfaces. Therefore, an ideal sputtering condition should achieve uniform sputtering yields across all materials in the sample while minimizing induced roughness at the crater bottom.

The two different GCIB sputter conditions were evaluated on pure MoO_3 and NPD films, each 50 nm in thickness, deposited upon a planar silicon wafer. The obtained sputtering yields are reported in Table 1.

It must be noted that the reported sputtering yields for MoO_3 should be considered as average values for a material whose stoichiometry evolves with increasing fluence (Fig. S1). Indeed, it is known that under monoatomic ion beam sputtering, molybdenum oxide undergoes reduction, due to the preferential removal of oxygen atoms [12,13], resulting in the formation of a sub-stoichiometric oxide, with consequent molybdenum enrichment of the sample surface. Similar behaviors have been reported, under Ar-GCIB bombardment, for analogous oxides such as NbO_X [32]. In our case, combined XPS-Ar-GCIB measurements show that MoO_3 undergoes reduction during sputtering in conditions similar to those adopted for SIMS depth profiling (Fig. 2).

Regardless of this behavior, by looking at the values reported in Table 1, as expected [32,35], the use of higher energy per incident atom results in an increased sputtering yield of the inorganic material. In fact, the average sputtering yield of MoO_3 increases from 1.3 nm^3/PI found under Ar^+_{4000} 20 keV (5 eV/n) to 5.8 nm^3/PI under Ar^+_{500} 20 keV (40 eV/n) bombardment, i.e. nearly a factor five.

By contrast, in the case of NPD the sputtering yield with 20 keV Ar^+_{4000} exceeds by a factor of more than two the value obtained with 20 keV Ar^+_{500}. This finding apparently contradicts the previsions of the "universal" curve reported by Seah, but it can be explained with the presence of some damage of the NPD layer under the higher energy per atom irradiation, similarly to what is known to happen when attempting to profile with C^+_{60} primary ion organic or polymer systems that undergo extensive damage [28]. In any case, according to Table 1, as the energy per atom increases from 5 eV to 40 eV, it is possible to reduce the sputtering yield difference between MoO_3 and NPD, with a decrease of about one order of magnitude of the Y_{NPD}/Y_{MoO3} ratio.

In the context of efficient SIMS characterization of hybrid materials, it is considered optimal to ensure that the sputtering yield for all materials is as uniform as possible. This is to minimize artifacts, and more importantly, to effectively erode all components of the specimen. In this regard, the 40 eV/n beam has been identified as a more promising analytical tool for the study of the NPD/MoO_3 hybrid system.

It is also crucial to consider that, in selecting the dimension and energy of the primary cluster ions, the sputtering yield ratio must be considered alongside other parameters, such as the retention of the molecular information from the organic component of the hybrid system.

In the case of organic samples, one expects that the molecular information is better preserved at lower energies/atom. This, in turn, is expected to enhance the probability of sampling an intact molecule from beneath the surface, as fewer impacts are necessary to remove the overlying material, thus mitigating the damage accumulation process [48]. For this reason, following the assessment of the 40 eV/n condition as effective in the erosion of the inorganic moiety, and with the objective of the characterization of a layered hybrid system, we evaluated the

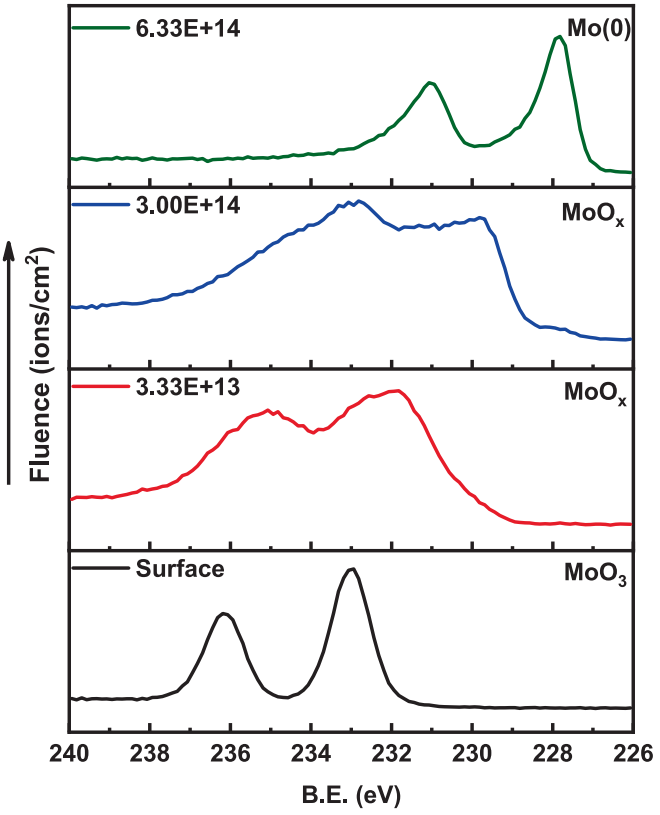

Fig. 2. Effect of 20 keV Ar^+_{620} irradiation on MoO_3 film (Fig. 1b), following the Mo3d XPS signal. The surface spectrum (black line) shows a binding energy of 232.9 eV for Mo $3d_{5/2}$, in agreement with literature values for Mo(VI) [44–46]. The broad range of B.E.'s labelled as MoO_x approximately indicates the expected position of bands due to the presence of suboxides due to beam-induced reduction. After a fluence of 6.33 × 10^{14} ions/cm^2 a calculated binding energy of 227.7 eV for Mo $3d_{5/2}$ appears, in accordance with the literature value for Mo (0) [47].

Table 1
Sputtering yield of NPD and MoO_3 obtained with Ar^+_{4000} 20 keV, Ar^+_{500} 20 KeV. The last column shows the ratio between sputtering yields of the two pure materials for each sputter beam.

	Y_{NPD}	Y_{MoO_3}	$\frac{Y_{NPD}}{Y_{MoO_3}}$
Ar^+_{4000} 20 keV (5 eV/n)	162 ± 7 nm^3/PI	1.3 ± 0.1 nm^3/PI	124.6
Ar^+_{500} 20 keV (40 eV/n)	74 ± 9 nm^3/PI	5.8 ± 1 nm^3/PI	12.7

efficacy of this experimental condition in preventing damage accumulation during sputtering of the pure organic material, i.e. NPD, throughout the SIMS depth profiling experiment. Fig. 3 reports the ToF-SIMS depth profile of the NPD layer deposited on silicon, obtained with Ar^+_{500} 20 keV (40 eV/n), where $C_{44}H_{32}N_2^+$ (molecular ion, $[M]^+$), $C_{16}H_{11}N^+$ (an intense characteristic fragment) and Si_2^+ (from substrate) are reported. The $[M]^+$ signal (*m/z* 588) exhibits an initial exponential intensity decay at low primary ion fluence, with a change in slope occurring at approximately 1×10^{13} ions/cm^2, where a "pseudo" steady state [37] is achieved and maintained until the interface with the substrate is reached. A similar trend is observed for the $C_{16}H_{11}N^+$ characteristic fragment, which however tends to increase its relative intensity, compared to $[M]^+$, after the very initial part of the profile. These observations indicate that the organic material can be regarded as "pristine" at low fluence, while at higher fluence a certain alteration of the molecular structure is induced, resulting in a more pronounced $[M]^+$ intensity decay compared to $C_{16}H_{11}N^+$ characteristic fragment intensity. As sputtering continues, the fraction of chemical damaged subsurface molecules increases eventually reaching a saturation point [48], where the pseudo steady state appears [37,49]. Noticing, despite the utilization of sputtering parameters that are not conventionally considered optimal for the profiling of molecular organic materials, the molecular signal of NPD was effectively detected and preserved across the entire thickness of the layer.

Looking at the depth profile reported in Fig. 3, we observe the presence of a broad interface with the substrate centered at about 6×10^{13} ions/cm^2, in contrast with what was observed on the same layer eroded with a lower eV/n beam (Fig. S2 a). Such a broad interface might suggest, among others, the presence of a rather high roughness at the interface.

To investigate this hypothesis, AFM measurements were conducted both prior to and during the SIMS depth profiling on NPD. These measurements provided insight into the evolution of beam-induced surface roughness. Prior to sputtering (Fig. 4a) the NPD sample revealed an average roughness (R_{RMS}) of 0.25 nm at the top surface, indicating a highly smooth morphology consistent with the typical results of physical vapor deposition (PVD) technique employed for material deposition. In contrast, the R_{RMS} measured for a sputtered crater obtained with Ar^+_{500} at 20 keV and stopped at a fluence of $\sim 1.5 \times 10^{13}$ ions/cm^2 was 2.56 nm (Fig. 4b), while the R_{RMS} measured when using Ar^+_{4000} 20 keV was only 0.92 nm (Fig. S2 b). This substantial increase in surface roughness suggests that the applied sputtering condition induces not only chemical but also morphological damage. The second one is responsible for the broad interface observed in the depth profile, since areas still containing NPD and areas already showing the silicon substrate are being simultaneously eroded in the same sputter frame [50–53].

These preliminary investigations comparing the performance of Ar^+_{500} 20 keV (40 eV/n) to a lower energy per atom sputtering regime (Ar^+_{4000} 20 keV, 5 eV/n) demonstrate that the higher energy condition significantly reduces the sputtering yield disparity between the organic and inorganic components to approximately one order of magnitude, as shown in Table 1. This improvement helps mitigate potential instrumental artifacts associated with the use of sputtering conditions poorly suited for inorganic materials, like Ar^+_{4000} 20 keV, which may erode different sample components at incompatible rates, as demonstrated from the partial depth profile shown in Fig. S3. Despite the known risk of partial chemical or morphological damage to the organic phase under high-energy conditions, it is noteworthy that the molecular information from NPD was preserved down to the silicon substrate. These findings highlight Ar^+_{500} 20 keV as a promising compromise, balancing the need for efficient erosion of the inorganic matrix with the preservation of molecular integrity in the organic component. Based on these results, this condition was selected for further investigation into the model layered hybrid system.

Fig. 5 reports a depth profile, obtained in dual beam mode by using such cluster beam for sputtering and a Bi_3^+ beam for analysis, of a structure wherein the organic layer is sandwiched between the silicon substrate and a top layer of MoO_3. The characteristic ions MoO_2^+ (*m/z* 130) and Mo^+ (*m/z* 98) were selected to represent the MoO_3 layer while the NPD layer is represented in figure by $C_{44}H_{32}N_2^+$ (molecular ion, $[M]^+$) and by C^+ ion (chosen as non-specific marker of the organic layer). The silicon substrate region can be identified by the Si_2^+ ion.

The MoO_2^+ signal delineates the 10 nm layer of MoO_3, with an interface with NPD identified at $\sim 2 \times 10^{13}$ ions/cm^2. The Mo^+ signal exhibits a maximum shifted to a higher fluence than MoO_2^+, consistent with the MoO_3 reduction upon ion beam bombardment. Simultaneously, the $C_{44}H_{32}N_2^+$ signal intensity rapidly increases before beginning a rapid decay, failing to reach a steady state and reaching the background intensity level much before the silicon interface, which is somehow marked by the Si_2^+ rise. This complicates the identification of the NPD layer region and the precise determination of the NPD/Si interface, which can be detected by tracking the non-specific C^+ ion or, as stated above, by means of the substrate signal.

The observed behavior of the $[M]^+$ signal is consistent with a

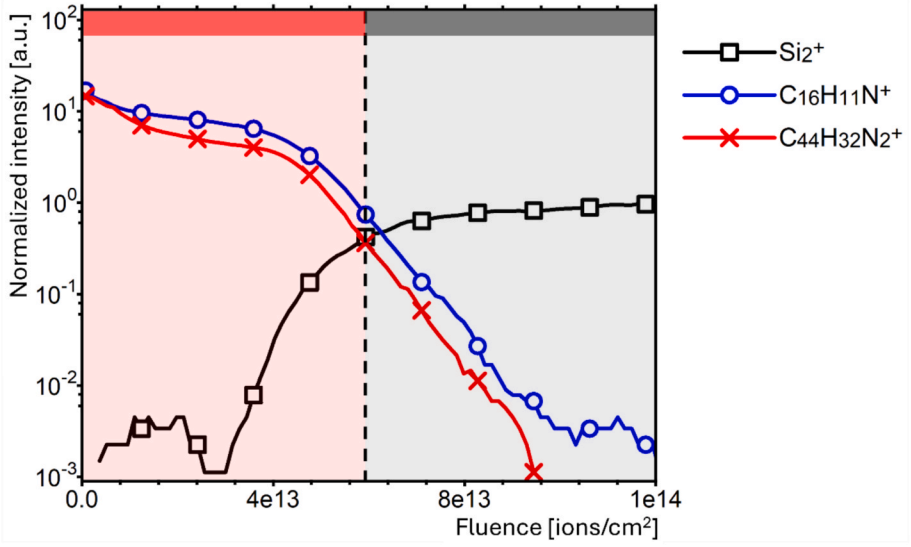

Fig. 3. NPD film (Fig. 1c) depth profile acquired with Ar^+_{500} 20 keV. The two regions, NPD, and silicon substrate, are indicated by the red and gray boxes, respectively. The dashed line qualitatively marks the interface. Intensities are normalized to the steady state value of the substrate signal Si_2^+.

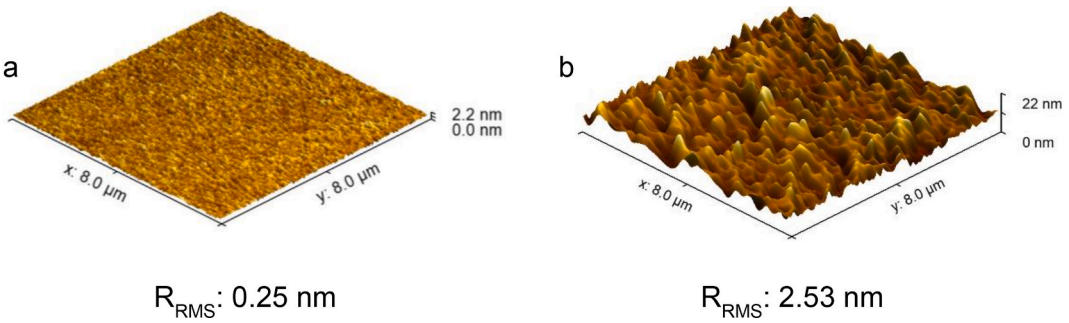

Fig. 4. AFM images and average roughness of the NPD film during cluster-SIMS depth profiling: a) top surface (no irradiation); b) crater bottom after stopping the depth profiling at a fluence of ~ 1.5×10^{13} ions/cm^2 with Ar_{500}^+ 20 keV.

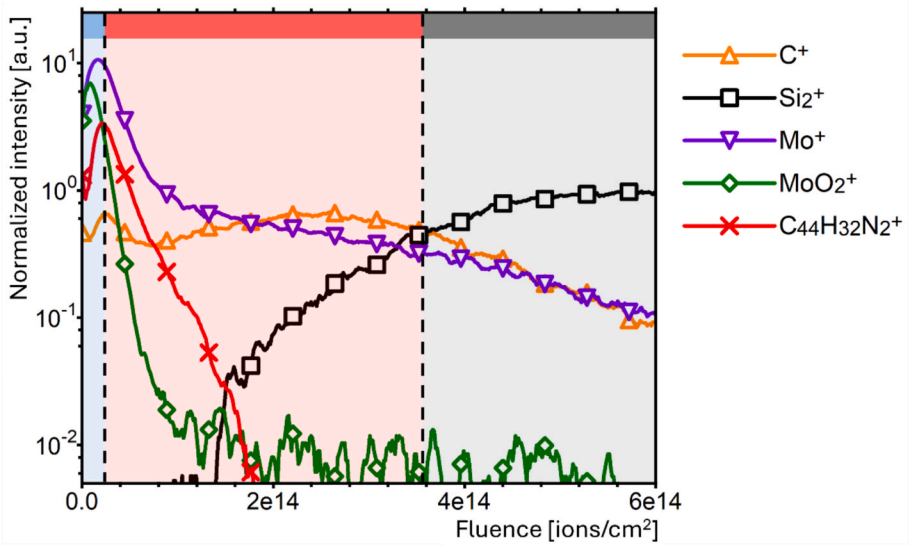

Fig. 5. MoO_3/NPD film (Fig. 1d) depth profile, acquired with Ar_{500}^+ 20 keV. The three regions, MoO_3, NPD, and the silicon substrate, are indicated by the blue, red and gray boxes, respectively. The dashed lines qualitatively mark the interfaces. Intensities are normalized to the steady state value of the substrate signal Si_2^+.

chemical damage process [54–57], where ion-sample interactions generate reactive species (presumably free radicals) that rapidly undergo reactions (such as crosslinking, rearrangement or decomposition reactions) [58], resulting in the loss of molecular information. Although some ion-induced reaction mechanisms have been investigated in polymers such as polystyrene or PMMA, as first approximation it is reasonable to extend the applicability of the concept of ion-beam induced reactions to an organic molecular solid such as NPD.

It is interesting to observe that, while in depth profile of pure NPD acquired in the same conditions (Fig. 3) it is possible to follow $[M]^+$ down to the substrate, in this case the molecular signal disappears well before. Additionally, while in case of Fig. 3 a fluence of ~ 4×10^{13} ions/cm^2 is sufficient to erode 50 nm of NPD deposited on silicon, in this case the NPD/Si interface is identified at ~ 4×10^{14} ions/cm^2, indicating a marked reduction of the sputtering yield. Also, such a decrease in sputtering yield suggests the presence of damage accumulation, in analogy to the case of polymer systems where extensive damage corresponds to lower sputtering yields. Since the selected operational condition alone cannot account for the observed phenomenon, an additional reason must be considered.

In the literature, similar damage effects have been described in the case of other organic layers underlying a metal film, depth profiled using low energy Cs^+ [18], or C_{60}^+ [39,59]. It has been hypothesized that, as a consequence of ion bombardment, metal penetration occurs within the organic layer, and this is thought to produce increased damage of the organic system. This hypothesis is consistent with the results of Kennedy et al. [60] who performed a molecular dynamics (MD) simulation of a silver/octatetraene hybrid interface bombarded with a C_{60} cluster beam. The simulation shows that a complex phenomenology occurs when the metal overlayer thickness is small enough to allow part of the beam energy to be deposited in the underlying organic layer. This occurs with the formation of holes in the metal overlayers, the pushing of metal atoms and metal clusters inside the organic film and ion mixing in the organic material. According to the authors [60], "the larger information depth, the larger displacements, and the altered physical and chemical environment are the main reasons for the poor ability to depth profile through a metal–organic interface".

Regardless of the detailed mechanism connected to the presence of the top inorganic layer, the chemical damage leading to the loss of molecular information is thought to be a kinetically driven process [28,41]. In this assumption we can hypothesize that temperature changes could interfere with the damage process by modifying the reactivity of transient active species (such as radicals) responsible for the ion-beam induced damage reactions. Therefore, to investigate the effect of temperature variation on the preservation of molecular information from the buried organic layer, a depth profile analysis at 148 K using Ar_{500}^+ at 20 keV (Fig. 6) was conducted on the bilayer.

Fig. 6 shows that depth profiling at low temperature preserves the $[M]^+$ signal nearly down to the silicon substrate. Furthermore, the silicon interface is reached at a fluence of ~ 2×10^{14} ions/cm^2, which is approximately half of the fluence required to reach the same interface in the depth profile experiment conducted at room temperature (Fig. 5).

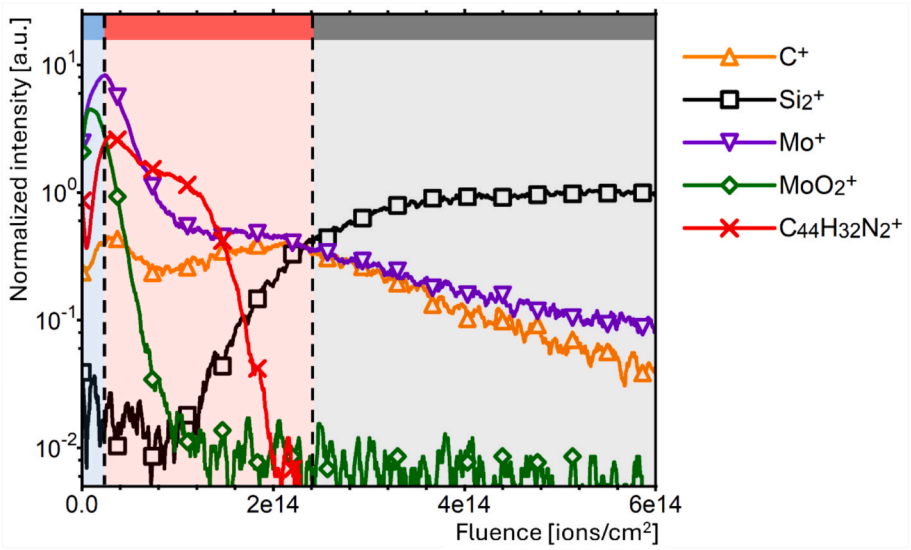

Fig. 6. MoO_3/NPD film (Fig. 1d) depth profile, acquired with Ar^+_{500} 20 keV at 148 K. The three regions, MoO_3, NPD, and the silicon substrate, are indicated by the blue, red and gray boxes, respectively. The dashed lines qualitatively mark the interfaces. Intensities are normalized to the steady state value of the substrate signal Si^+_2.

The increased erosion rate is associated with diminished damage accumulation, thereby better preserving the pristine material chemical properties. This observation suggests that the primary sources of sample damage arise from ion-induced chemical reactions and ion beam mixing processes at the organic region, as evidenced by the depth profile acquired at room temperature. In this context, the reactive species generated by the fragmentation of NPD molecules are likely to be kinetically immobilized, preventing them from reacting within the experimental timescale. This reduction of reactivity decreases the damage rate and allows for the preservation of molecular information throughout nearly the entire material thickness, while still being able to perform depth profiling on the inorganic counterpart.

Noticeably, even at lower temperatures, the signals originating from MoO_3 layer exhibit the same trend observed at room temperature, including the persistence of Mo^+ signal through the underlying organic layer. In other words, the temperature reduction does not affect directly the ion beam mixing process, which – most likely – remains essentially a ballistic process, but interferes with the reactive transient species at the buried organic layer, generated upon the above-mentioned ion beam mixing process. On the other hand, the low temperature slows down the rate of the reactions involving the active species produced by the beam (including those potentially produced by the penetration of metal atoms in the organic layer) therefore inhibiting the occurrence of mechanisms, such as crosslinking, that contribute to the damage and thereby mitigating the loss of molecular information.

4. Conclusions

This study demonstrates the beneficial effects of decreasing sample temperature during dual beam SIMS depth profiling of layered hybrid samples in combination with the use of high-energy-per-atom argon cluster beams. By selecting smaller clusters with higher impact energies, compared to the typical values employed in cluster beam sputtering of all-organic samples, it is possible to reduce the disparity in sputtering yield between the inorganic (MoO_3) and the organic (NPD) materials while preserving, to some extent, the molecular information.

However, when acquiring depth profiles on layered hybrid systems where the inorganic layer is situated on top of the organic one, severe chemical damage of the organic layer is observed. This results in the loss of molecular information and a reduction of the sputtering yield of such a layer. We hypothesized that the processes responsible for such damage are kinetically driven. To verify this hypothesis, temperature-assisted depth profiles were performed. Specifically, the results demonstrated that reducing the sample temperature to 148 K appeared to be sufficient to "freeze" the reactive species responsible for the loss of molecular information in the NPD organic layer, thereby preserving the characteristic ion signals from the organic material and ensuring the successful characterization of layered hybrid system. The approach proposed in this study paves the way for the investigation of more complex hybrid structures, providing a reliable and straightforward method for their characterization. The focus of future studies will be to explore and investigate the potential of this approach when it is applied to blends of organic and inorganic materials, as well as stacks of different organic and inorganic materials.

Fundings

Author V.S. would like to acknowledge the MetTriPI (Metodologie avanzate per la caratterizzazione chimico fisica Tridimensionale di sistemi Polimerici ed Ibridi) project, founded by PIano di inCEntivi per la RIcerca (PIACERI) 2020/2022, Linea di Intervento 3 "Starting Grant", Università degli Studi di Catania, for financial support. Authors N.T. and V.S. would like to acknowledge the SUPERMOL project, funded under the National Recovery and Resilience Plan (NRRP), Mission 4 Component 2 Investment 1.3 – call for tender No. 1561 of 11.10.2022 of Ministero dell'Università e della Ricerca (MUR); funded by the European Union – NextGenerationEU, Project code PE0000021 – CUP B53C22004060006 – "SUPERMOL", "Network 4 Energy Sustainable Transition – NEST"). Authors G.R., A.B. and A.L. would like to acknowledge PRIN 2022 project "MEET" (project code 20225P4EJC, CUP E53D23008350006), Author M.P. would like to acknowledge PRIN 2022 project "FUTURO" (project code 2022FWZCHK, CUP B53D23013680006). The PRIN 2022 projects were funded under the National Recovery and Resilience Plan (NRRP), Mission 4, Component 2, Investment 1.1, call for tender No. 104 of 2.2.2022 of Italian Ministry of University and Research (MUR), funded by the European Union – NextGenerationEU.

CRediT authorship contribution statement

Giuseppe Ragusano: Writing – review & editing, Writing – original draft, Visualization, Validation, Methodology, Investigation, Data

curation, Conceptualization. **Valentina Spampinato:** Writing – review & editing, Supervision, Project administration, Methodology, Funding acquisition, Conceptualization. **Alessandro Auditore:** Writing – review & editing, Supervision, Methodology, Investigation, Conceptualization. **Nunzio Tuccitto:** Writing – review & editing, Methodology, Funding acquisition, Conceptualization. **Marta Penconi:** Writing – review & editing, Resources, Funding acquisition. **Alberto Bossi:** Writing – review & editing, Resources, Funding acquisition. **Alexis Franquet:** Writing – review & editing, Resources. **Thierry Conard:** Writing – review & editing, Resources. **Antonino Licciardello:** Writing – review & editing, Supervision, Resources, Methodology, Funding acquisition, Conceptualization.

Declaration of competing interest

The authors declare that they have no known competing financial interests or personal relationships that could have appeared to influence the work reported in this paper.

Appendix A. Supplementary data

Supplementary data to this article can be found online at https://doi.org/10.1016/j.apsusc.2025.164456.

Data availability

Data will be made available on request.

References

[1] P. Gomez-Romero, A. Pokhriyal, D. Rueda-García, L.N. Bengoa, R.M. González-Gil, Hybrid materials: a metareview, Chem. Mater. 36 (2024) 8–27, https://doi.org/10.1021/acs.chemmater.3c01878.

[2] S.H. Wu, M.F. Lo, Z.Y. Chen, T.W. Ng, X. Hu, H.W. Mo, C. Wu, W.L. Li, C.S. Lee, Simple near-infrared photodetector based on charge transfer complexes formed in molybdenum oxide doped N,N′-di(naphthalene-1-yl)-N,N′-diphenyl-benzidine, Phys. Status Solidi (RRL) – Rapid Res. Lett. 6 (2012) 129–131. Doi: 10.1002/pssr.201105596.

[3] H. Wang, S. Liu, Y. Li, X. Yue, Y. Shen, H. Xu, H. Xu, Y. Tan, L. Zeng, B. Yao, Z. Fang, Near-infrared-II photodetection realized by introducing organic-inorganic charge-transfer-complex photosensitive material into pentacene phototransistor, Org. Electron. 77 (2020) 105500, https://doi.org/10.1016/j.orgel.2019.105500.

[4] A. Lee, J.D. Lichtenhan, Viscoelastic responses of polyhedral oligosilsesquioxane reinforced epoxy systems, Macromolecules 31 (1998) 4970–4974, https://doi.org/10.1021/ma9800764.

[5] M.P. de Jong, L.J. van IJzendoorn, M.J.A. de Voigt, Stability of the interface between indium-tin-oxide and poly(3,4-ethylenedioxythiophene)/poly (styrenesulfonate) in polymer light-emitting diodes, Appl. Phys. Lett. 77 (2000) 2255–2257, https://doi.org/10.1063/1.1315344.

[6] M. Penconi, M. Cazzaniga, W. Panzeri, A. Mele, F. Cargnoni, D. Ceresoli, A. Bossi, Unraveling the degradation mechanism in firpic-based blue OLEDs: II. Trap and detect molecules at the interfaces, Chem. Mater. 31 (2019) 2277–2285, https://doi.org/10.1021/acs.chemmater.8b04502.

[7] J. Han, H. Xu, S.H.K. Paleti, A. Sharma, D. Baran, Understanding photochemical degradation mechanisms in photoactive layer materials for organic solar cells, Chem. Soc. Rev. 53 (2024) 7426–7454, https://doi.org/10.1039/D4CS00132J.

[8] P.K. Chu, SIMS and microelectronics, Mater. Chem. Phys. 38 (1994) 203–223, https://doi.org/10.1016/0254-0584(94)90195-3.

[9] S. Netcheva, P. Bertrand, Ion-beam-induced morphology on the surface of thin polymer films at low current density and high ion fluence, J. Polym. Sci. B Polym. Phys. 39 (2001) 314–325, https://doi.org/10.1002/1099-0488(20010201)39:3<314::AID-POLB1003>3.0.CO;2-6.

[10] A. Chilkoti, G.P. Lopez, B.D. Ratner, M.J. Hearn, D. Briggs, Analysis of polymer surfaces by SIMS. 16. Investigation of surface crosslinking in polymer gels of 2-hydroxyethyl methacrylate, Macromolecules 26 (1993) 4825–4832.

[11] M. Saggio, C. Montandon, A. Bourenkov, L. Frey, P. Pichler, Distortion of SIMS profiles due to ion beam mixing, Radiat Eff. Defects Solids 141 (1997) 37–52, https://doi.org/10.1080/10420159708211555.

[12] H.M. Naguib, R. Kelly, On the increase in the electrical conductivity of MoO3 and V2O5 following ion bombardment. Studies on bombardment-enhanced conductivity-I, J. Phys. Chem. Solid 33 (1972) 1751-IN5, https://doi.org/10.1016/S0022-3697(72)80469-4.

[13] R. Kelly, N.Q. Lam, The sputtering of oxides part i: a survey of the experimental results, Radiat. Eff. 19 (1973) 39–48, https://doi.org/10.1080/00337577308232213.

[14] J.B. Malherbe, S. Hofmann, J.M. Sanz, Preferential sputtering of oxides: a comparison of model predictions with experimental data, Appl. Surf. Sci. 27 (1986) 355–365, https://doi.org/10.1016/0169-4332(86)90139-X.

[15] G. Gillen, S. Roberson, Preliminary evaluation of an SF5+ polyatomic primary ion beam for analysis of organic thin films by secondary ion mass spectrometry, Rapid Commun. Mass Spectrom. 12 (1998) 1303–1312, https://doi.org/10.1002/(SICI)1097-0231(19981015)12:19<1303::AID-RCM330>3.0.CO;2-7.

[16] A. Benninghoven, D. Jaspers, W. Sichtermann, Secondary-ion emission of amino acids, Appl. Phys. 11 (1976) 35–39, https://doi.org/10.1007/BF00895013.

[17] F. Kötter, A. Benninghoven, Secondary ion emission from polymer surfaces under Ar+, Xe+ and SF5+ ion bombardment, Appl. Surf. Sci. 133 (1998) 47–57, https://doi.org/10.1016/S0169-4332(97)00515-1.

[18] C. Noël, L. Houssiau, Hybrid organic/inorganic materials depth profiling using low energy cesium ions, J. Am. Soc. Mass Spectrom. 27 (2016) 908–916, https://doi.org/10.1007/s13361-016-1353-9.

[19] C. Noël, Y. Busby, N. Mine, L. Houssiau, ToF-SIMS depth profiling of organic delta layers with low-energy cesium ions: depth resolution assessment, J. Am. Soc. Mass Spectrom. 30 (2019) 1537–1544, https://doi.org/10.1007/s13361-019-02224-4.

[20] L. Houssiau, N. Mine, Molecular depth profiling with reactive ions, or why chemistry matters in sputtering, Surf. Interface Anal. 43 (2011) 146–150, https://doi.org/10.1002/sia.3528.

[21] C. Noël, N. Tuccitto, Y. Busby, M. Auer-Berger, A. Licciardello, E.J.W. List-Kratochvil, L. Houssiau, Depth profiling of organic light-emitting diodes by ToF-SIMS coupled with wavelet–principal component analysis, ACS Appl. Polym. Mater. 1 (2019) 1821–1828, https://doi.org/10.1021/acsapm.9b00292.

[22] T. Terlier, G. Zappalà, C. Marie, D. Leonard, J.-P. Barnes, A. Licciardello, ToF-SIMS depth profiling of PS-b-PMMA block copolymers using Arn+, C60++, and Cs+ sputtering ions, Anal. Chem. 89 (2017) 6984–6991, https://doi.org/10.1021/acs.analchem.7b00279.

[23] T. Mouhib, C. Poleunis, N. Wehbe, J.J. Michels, Y. Galagan, L. Houssiau, P. Bertrand, A. Delcorte, Molecular depth profiling of organic photovoltaic heterojunction layers by ToF-SIMS: comparative evaluation of three sputtering beams, Analyst 138 (2013) 6801–6810, https://doi.org/10.1039/C3AN01035J.

[24] A. Geiser, B. Fan, H. Benmansour, F. Castro, J. Heier, B. Keller, K.E. Mayerhofer, F. Nüesch, R. Hany, Poly(3-hexylthiophene)/C60 heterojunction solar cells: Implication of morphology on performance and ambipolar charge collection, Sol. Energy Mater. Sol. Cells 92 (2008) 464–473, https://doi.org/10.1016/j.solmat.2007.11.001.

[25] D. Stapel, O. Brox, A. Benninghoven, Secondary ion emission from arachidic acid LB-layers under Ar+, Xe+, Ga+ and SF5+ primary ion bombardment, Appl. Surf. Sci. 140 (1999) 156–167, https://doi.org/10.1016/S0169-4332(98)00584-4.

[26] D. Weibel, S. Wong, N. Lockyer, P. Blenkinsopp, R. Hill, J.C. Vickerman, A C_{60} primary ion beam system for time of flight secondary ion mass spectrometry: its development and secondary ion yield characteristics, Anal. Chem. 75 (2003) 1754–1764, https://doi.org/10.1021/ac026338o.

[27] C. Szakal, S. Sun, A. Wucher, N. Winograd, C60 molecular depth profiling of a model polymer, Appl. Surf. Sci. 231–232 (2004) 183–185, https://doi.org/10.1016/j.apsusc.2004.03.113.

[28] R. Möllers, N. Tuccitto, V. Torrisi, E. Niehuis, A. Licciardello, Chemical effects in C60 irradiation of polymers, Appl. Surf. Sci. 252 (2006) 6509–6512, https://doi.org/10.1016/j.apsusc.2006.02.083.

[29] S. Ninomiya, K. Ichiki, H. Yamada, Y. Nakata, T. Seki, T. Aoki, J. Matsuo, Precise and fast secondary ion mass spectrometry depth profiling of polymer materials with large Ar cluster ion beams, Rapid Commun. Mass Spectrom. 23 (2009) 1601–1606, https://doi.org/10.1002/rcm.4046.

[30] D. Rading, R. Moellers, H.-G. Cramer, E. Niehuis, Dual beam depth profiling of polymer materials: comparison of C_{60} and Ar cluster ion beams for sputtering, Surf. Interface Anal. 45 (2013) 171–174, https://doi.org/10.1002/sia.5122.

[31] C.M. Mahoney, Cluster Secondary Ion Mass Spectrometry: Principles and Applications, John Wiley & Sons, 2013.

[32] A.A. Ellsworth, C.N. Young, W.F. Stickle, A.V. Walker, New horizons in sputter depth profiling inorganics with giant gas cluster sources: Niobium oxide thin films, Surf. Interface Anal. 49 (2017) 991–999, https://doi.org/10.1002/sia.6259.

[33] S. Ninomiya, K. Ichiki, Y. Nakata, T. Seki, T. Aoki, J. Matsuo, The effect of incident cluster ion energy and size on secondary ion yields emitted from Si, Nucl. Instrum. Methods Phys. Res. B 256 (2007) 528–531, https://doi.org/10.1016/j.nimb.2006.12.074.

[34] Y.K. Kyoung, H.I. Lee, J.G. Chung, S. Heo, J.C. Lee, Y.J. Cho, H.J. Kang, Damage profiles of Si (001) surface via Ar cluster beam sputtering, Surf. Interface Anal. 45 (2013) 150–153, https://doi.org/10.1002/sia.4917.

[35] M.P. Seah, Universal equation for argon gas cluster sputtering yields, J. Phys. Chem. C 117 (2013) 12622–12632, https://doi.org/10.1021/jp402684c.

[36] L. Yang, M.P. Seah, I.S. Gilmore, Sputtering yields for gold using argon gas cluster ion beams, J. Phys. Chem. C 116 (2012) 23735–23741, https://doi.org/10.1021/jp307203f.

[37] C.M. Mahoney, A.J. Fahey, G. Gillen, Temperature-controlled depth profiling of poly(methyl methacrylate) using cluster secondary ion mass spectrometry. 1. investigation of depth profile characteristics, Anal. Chem. 79 (2007) 828–836, https://doi.org/10.1021/ac061356h.

[38] C.M. Mahoney, A.J. Fahey, G. Gillen, C. Xu, J.D. Batteas, Temperature-controlled depth profiling of poly(methyl methacrylate) using cluster secondary ion mass spectrometry. 2. Investigation of sputter-induced topography, chemical damage, and depolymerization effects, Anal. Chem. 79 (2007) 837–845, https://doi.org/10.1021/ac061357+.

[39] K. Shen, D. Mao, B.J. Garrison, A. Wucher, N. Winograd, Depth profiling of metal overlayers on organic substrates with cluster SIMS, Anal. Chem. 85 (2013) 10565–10572, https://doi.org/10.1021/ac402658r.
[40] C. Noël, S. Pescetelli, A. Agresti, A. Franquet, V. Spampinato, A. Felten, A. di Carlo, L. Houssiau, Y. Busby, Hybrid perovskites depth profiling with variable-size argon clusters and monatomic ions beams, Materials 12 (2019) 726, https://doi.org/10.3390/ma12050726.
[41] G. Zappalà, V. Motta, N. Tuccitto, S. Vitale, A. Torrisi, A. Licciardello, Nitric oxide assisted C_{60} secondary ion mass spectrometry for molecular depth profiling of polyelectrolyte multilayers, Rapid Commun. Mass Spectrom. 29 (2015) 2204–2210, https://doi.org/10.1002/rcm.7383.
[42] N. Tuccitto, D. Maciazek, Z. Postawa, A. Licciardello, MD-based transport and reaction model for the simulation of SIMS depth profiles of molecular targets, J. Phys. Chem. C 123 (2019) 20188–20194, https://doi.org/10.1021/acs.jpcc.9b01653.
[43] V. Spampinato, M. Dialameh, A. Franquet, C. Fleischmann, T. Conard, P. van der Heide, W. Vandervorst, A correlative ToF-SIMS/SPM methodology for probing 3D devices, Anal. Chem. 92 (2020) 11413–11419, https://doi.org/10.1021/acs.analchem.0c02406.
[44] T.M. McEvoy, K.J. Stevenson, J.T. Hupp, X. Dang, Electrochemical preparation of molybdenum trioxide thin films: effect of sintering on electrochromic and electroinsertion properties, Langmuir 19 (2003) 4316–4326, https://doi.org/10.1021/la027020u.
[45] K. Du, W. Fu, R. Wei, H. Yang, J. Xu, L. Chang, Q. Yu, G. Zou, Ultrasonic-assisted synthesis of highly dispersed MoO3 nanospheres using 3-mercaptopropyltrimethoxysilane, Ultrason. Sonochem. 15 (2008) 233–238, https://doi.org/10.1016/j.ultsonch.2007.04.004.
[46] X. Fan, G. Fang, P. Qin, N. Sun, N. Liu, Q. Zheng, F. Cheng, L. Yuan, X. Zhao, Deposition temperature effect of RF magnetron sputtered molybdenum oxide films on the power conversion efficiency of bulk-heterojunction solar cells, J. Phys. D Appl. Phys. 44 (2011) 045101, https://doi.org/10.1088/0022-3727/44/4/045101.
[47] F. Werfel, E. Minni, Photoemission study of the electronic structure of Mo and Mo oxides, J. Phys. C Solid State Phys. 16 (1983) 6091–6100, https://doi.org/10.1088/0022-3719/16/31/022.
[48] Greg. Gillen, D.S. Simons, Peter. Williams, Molecular ion imaging and dynamic secondary-ion mass spectrometry of organic compounds, Anal. Chem. 62 (1990) 2122–2130, https://doi.org/10.1021/ac00218a014.
[49] A. Wucher, A simple erosion dynamics model of molecular sputter depth profiling, Surf. Interface Anal. 40 (2008) 1545–1551, https://doi.org/10.1002/sia.2933.
[50] M.A. Makeev, A.-L. Barabási, Effect of surface roughness on the secondary ion yield in ion sputtering, Appl. Phys. Lett. 73 (1998) 2209–2211, https://doi.org/10.1063/1.122425.
[51] M.A. Makeev, R. Cuerno, A.-L. Barabási, Morphology of ion-sputtered surfaces, Nucl. Instrum. Methods Phys. Res. B 197 (2002) 185–227, https://doi.org/10.1016/S0168-583X(02)01436-2.
[52] M.A. Makeev, A.-L. Barabási, Effect of surface morphology on the sputtering yields. I. Ion sputtering from self-affine surfaces, Nucl. Instrum. Methods Phys. Res. B 222 (2004) 316–334, https://doi.org/10.1016/j.nimb.2004.02.027.
[53] M.A. Makeev, A.-L. Barabási, Effect of surface morphology on the sputtering yields. II. Ion sputtering from rippled surfaces, Nucl. Instrum. Methods Phys. Res. B 222 (2004) 335–354, https://doi.org/10.1016/j.nimb.2004.02.028.
[54] A. Chapiro, Radiation chemistry of polymeric systems, Interscience Publishers (1962) 354.
[55] A. Chapiro, Radiation chemistry of polymers, Radiat. Res. Suppl. 4 (1964) 179, https://doi.org/10.2307/3583578.
[56] H. Dong, T. Bell, State-of-the-art overview: ion beam surface modification of polymers towards improving tribological properties, Surf. Coat. Technol. 111 (1999) 29–40, https://doi.org/10.1016/S0257-8972(98)00698-7.
[57] C.M. Mahoney, Cluster secondary ion mass spectrometry of polymers and related materials, Mass Spectrom. Rev. 29 (2010) 247–293, https://doi.org/10.1002/mas.20233.
[58] D.Y. Kondakov, Role of chemical reactions of arylamine hole transport materials in operational degradation of organic light-emitting diodes, J. Appl. Phys. 104 (2008), https://doi.org/10.1063/1.3006890.
[59] J. Cheng, N. Winograd, Molecular depth profiling of multi-layer systems with cluster ion sources, Appl. Surf. Sci. 252 (2006) 6498–6501, https://doi.org/10.1016/j.apsusc.2006.02.207.
[60] P.E. Kennedy, Z. Postawa, B.J. Garrison, Dynamics displayed by energetic C_{60} bombardment of metal overlayers on an organic substrate, Anal. Chem. 85 (2013) 2348–2355, https://doi.org/10.1021/ac303348y.